Journal of Structural Geology 30 (2008) 1072–1084

Contents lists available at ScienceDirect

Journal of Structural Geology

journal homepage: www.elsevier.com/locate/jsg

The kinematics of reactivation of normal faults using high resolution throw mapping

Catherine Baudon*, Joe Cartwright

3D Lab, School of Earth, Ocean and Planetary Sciences, Cardiff University, Main Building, Park Place, Cardiff CF10 3AT, UK

ARTICLE INFO

Article history:
Received 16 March 2007
Received in revised form 28 April 2008
Accepted 29 April 2008
Available online 8 May 2008

Keywords:
Fault reactivation
Upward propagation
Dip linkage
Throw distribution

ABSTRACT

Normal reactivation of extensional faults offsetting Cenozoic clastic sediments is investigated using high quality 3D seismic data from offshore Brazil. These faults form complex crestal collapse grabens and result from elliptical doming of the underlying Cretaceous sequence due to Early Cenozoic uplift. The exceptional quality of this dataset allows an extremely detailed analysis of the throw distribution to be conducted on the faults. This, in addition to a reconstruction of the 3D geometry of the fault network, gives insights into the mechanisms and kinematics of reactivation. Two distinct modes of reactivation are recognised from this dataset. The main mode is a classical reactivation by upward propagation of pre-existing structures. A second mode, termed reactivation by dip linkage, is the propagation of an individual fault segment initiated above the pre-existing faults that hard link in the dip direction. For both mechanisms, reactivation processes are selective and only occur on some portions of faults. Factors controlling the preferential reactivation of some segments include: (1) orientation of the pre-existing fault plane relative to the principal stresses responsible for the reactivation, (2) segmentation of the pre-existing network and (3) maximum dimensions and throw values of pre-existing faults and basal tip line geometry associated with a detachment. Reactivation is an important process that may account for part of the scatter in fault-scaling relationships and should be included in fault-growth models.

1. Introduction

Fault propagation has been investigated with seismic data, outcrop data, and analogue and numerical modelling, yielding a number of fault-growth models (e.g. Walsh and Watterson, 1988; Cowie and Scholz, 1992b; Cartwright et al., 1995). Reactivation processes have only recently been considered as an important control in fault propagation (Walsh et al., 2002; Bellahsen and Daniel, 2005). A better understanding of reactivation is essential to establish whether a fault is extinct or not (Muir Wood and Mallard, 1992), to better evaluate possible episodic fault activity (e.g. Blair and Bilodeau, 1988; Cartwright et al., 1998; Lisle and Srivastava, 2004) and to determine the effects of reactivation on fault-growth behaviour and scaling relationships (e.g. Cartwright et al., 1998; Meyer et al., 2002; Walsh et al., 2002; Nicol et al., 2005). Constraining reactivation processes has practical implications for improving the evaluation of seismic hazards (Lisle and Srivastava, 2004) and assessing the impact of reactivation on fault seal quality and fluid migration (Holdsworth et al., 1997).

Much previous work about reactivation has focused on originally extensional (e.g. Jackson, 1980; Kelly et al., 1999) or compressional (e.g. Brewer and Smythe, 1984; Enfield and Coward, 1987; Paton, 2006) fault systems that were inverted or reactivated in strike-slip mode (e.g. Kim et al., 2001). The vast majority of these studies consider faults that reactivated pre-existing basement structures, which is often seen as one of the major controls. Overall, it is still not really understood why some faults reactivate and others do not (e.g. Butler et al., 1997; Kelly et al., 1999).

This paper considers the case of a normal dip-slip system of crestal collapse faults that were subsequently affected by normal dip-slip reactivation. Additionally, the faults are not basement-rooted, so that factors controlling the reactivation are not limited to this inheritance. Using high quality 3D seismic data from offshore Brazil (Fig. 1), a detailed displacement analysis characterises the effects of reactivation on the throw distribution over the fault planes. The normal faults are interpreted to reactivate mostly by upward propagation but also by dip linkage with an overlying tier of normal faults. In addition to this behaviour, the factors influencing the selective reactivation are discussed given that not all faults are reactivated.

* Corresponding author. NARG, SEAES, The University of Manchester, Oxford Road, Williamson Building, Manchester, M13 9PL, UK. Tel.: +44 (0) 161 275 0778; fax.:+44 (0) 161 306 9361.
E-mail address: catherine.baudon@manchester.ac.uk (C. Baudon).

0191-8141/$ – see front matter © 2008 Elsevier Ltd. All rights reserved.
doi:10.1016/j.jsg.2008.04.008

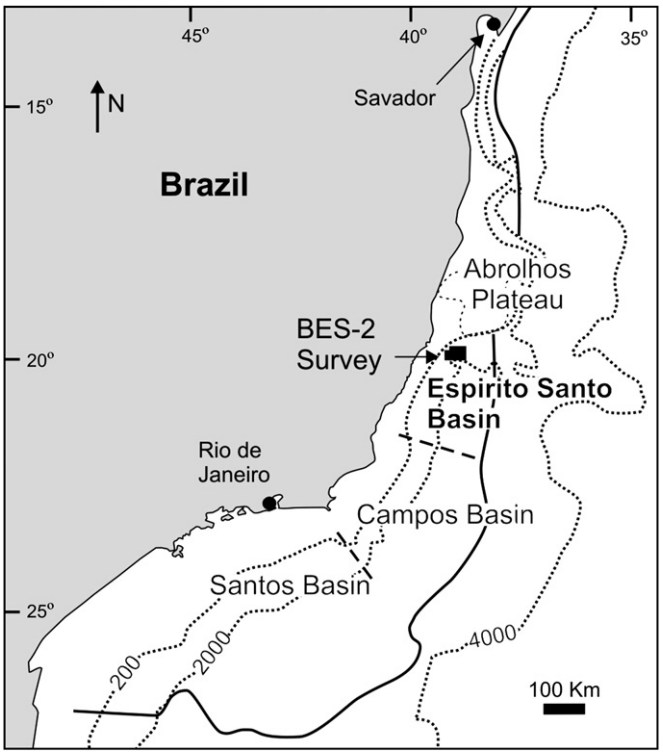

Fig. 1. Location of the BES-2 Survey in the Espirito Santo Basin, offshore Brazil (after Chang et al., 1992). Dotted lines indicate the bathymetry (m), dashed lines symbolise the limits between different basins and solid line indicates the margin of the evaporites.

2. Geological setting

The Espirito Santo Basin is located on the passive margin of Brazil, between the Campos Basin and the Abrolhos volcanic Plateau (Figs. 1 and 2), and was part of the east Brazil rift system that led to the opening of the Atlantic (e.g. Austin and Uchupi, 1982; Chang et al., 1992; Meisling et al., 2001). The syn-rift sediments (Late Berriasian to Early Aptian) are mainly continental sandstones, shales and syntectonic conglomerates that alternate with igneous material (Ojeda, 1982; Chang et al., 1992). A transitional stage of stable tectonic activity (Middle to Late Aptian) is characterised by thick layers of evaporitic sediments (Ojeda, 1982; Demercian et al., 1993). The drift phase corresponds to two main megasequences of deposition (Mohriak et al., 1998). These are: (1) an Albian marine-transgressive megasequence with shallow carbonate platforms overlain by marls and shales resulting from further deepening of the basin (Chang et al., 1992; Demercian et al., 1993), and (2) a Cenozoic marine-regressive megasequence that is the main interval of interest of this work and consists of prograding siliciclastic sediments derived from the erosion of coastal mountains (Chang et al., 1992). A major unconformity (Top K) separates the Mesozoic and Cenozoic megasequences (Fiduk et al., 2004).

Deformation in the Espirito Santo Basin was greatly influenced by gravity-driven salt-tectonics (Demercian et al., 1993; Fiduk et al., 2004). The structural style of the salt-cored structures changes across the basin, but vertical salt diapirs occurring along contractional folds dominate within the study area. Variation in stratal thickness with respect to these anticlines suggests that folding of the Cretaceous interval occurred in the early Cenozoic in the survey area. Most diapirs are still active and can be observed in close proximity to the present day seabed, but some became inactive during the Cenozoic. The movement of salt underlying the Cretaceous strata and the salt diapirs piercing through the Cenozoic sequence strongly influenced the location and geometry of the structures studied in this paper.

3. 3D seismic interpretation

3.1. Dataset

The BES-2 survey of 3D seismic data used in this study covers an area of c. 1600 km^2 within the Espirito Santo Basin in water depths ranging from c. 100 to 1800 m. The data are zero-phase migrated with 12.5 × 12.5 m inline and crossline spacing and the dominant frequency within the Cenozoic interval ranges from 35 to 60 Hz decreasing with depth. No velocity information was available for this dataset. An average velocity value of 1800 m s^{-1} was estimated from typical seismic velocity values of clastic sediments in various slope and deep-water settings and from analogy with shallow seismic sections in other basins of the Brazilian continental margin (Rodger et al., 2006). Vertical resolution within the interval of interest is c. 7–13 m, assuming such a velocity. Seismic data beneath 4 s TWT were not available for this study but the Cenozoic is the main interval of interest for this work (Fig. 2a). Regional key horizons and fault planes were mapped at different stratigraphic levels using Schlumberger Geoframe 3.7 seismic interpretation software. Detailed measurements of the throw values on faults were made using fault normal seismic profiles and displayed as individual vertical throw distribution plots (*T–z* plot) (Cartwright et al., 1998; Baudon and Cartwright, 2008).

3.2. Seismic stratigraphic framework

A few continuous and high amplitude seismic reflections mark the base of the Cenozoic sediments. Three main units were defined from differences in seismic characteristics (Fig. 3). Unit 1 overlies directly the top Cretaceous sediments in a discordant manner and is bounded at the top by an erosional unconformity, believed to be post middle Eocene to Oligocene (E–O) in age (Fiduk et al., 2004). Unit 1 is expressed as moderate amplitude and continuous seismic reflections and is separated into 2 sub-units. Unit 1a (Top K to C60) thins above the anticlines as a result of syn-tectonic deposition whereas Unit 1b (C60 to E–O boundary) forms an interval with no significant change in thickness. The basal part of Unit 2 consists, in most of the faulted areas of the survey, of a c. 100 m thick interval of chaotic seismic-facies that is interpreted as slump deposits. The base of the slump interval is expressed as an erosional truncation surface with respect to the underlying seismic reflections (Figs. 3 and 8b). The underlying strata are eroded over most of the survey and the upper tip lines of faults located in Unit 1 are truncated as a result of this erosion. Unit 2 shows a striking increase in seismic reflectivity with respect to the two surrounding units, due to a high proportion of volcani-clastic material derived from the Abrolhos Plateau (Fiduk et al., 2004). The overlying strata consist of continuous and high amplitude seismic reflections characteristic of siliciclastic material of lower slope facies alternating with a few c. 50 m thick intervals of chaotic facies interpreted as slump deposits. Unit 2 does not exhibit a significant change in thickness over the whole survey. Unit 3 overlies Unit 2 in a concordant manner and is bounded at the top by the seabed. It consists of a package of high-frequency continuous and moderate to high-amplitude seismic reflections. The overall thickness of this unit changes significantly where subsequent erosion occurred with channel complex deposition.

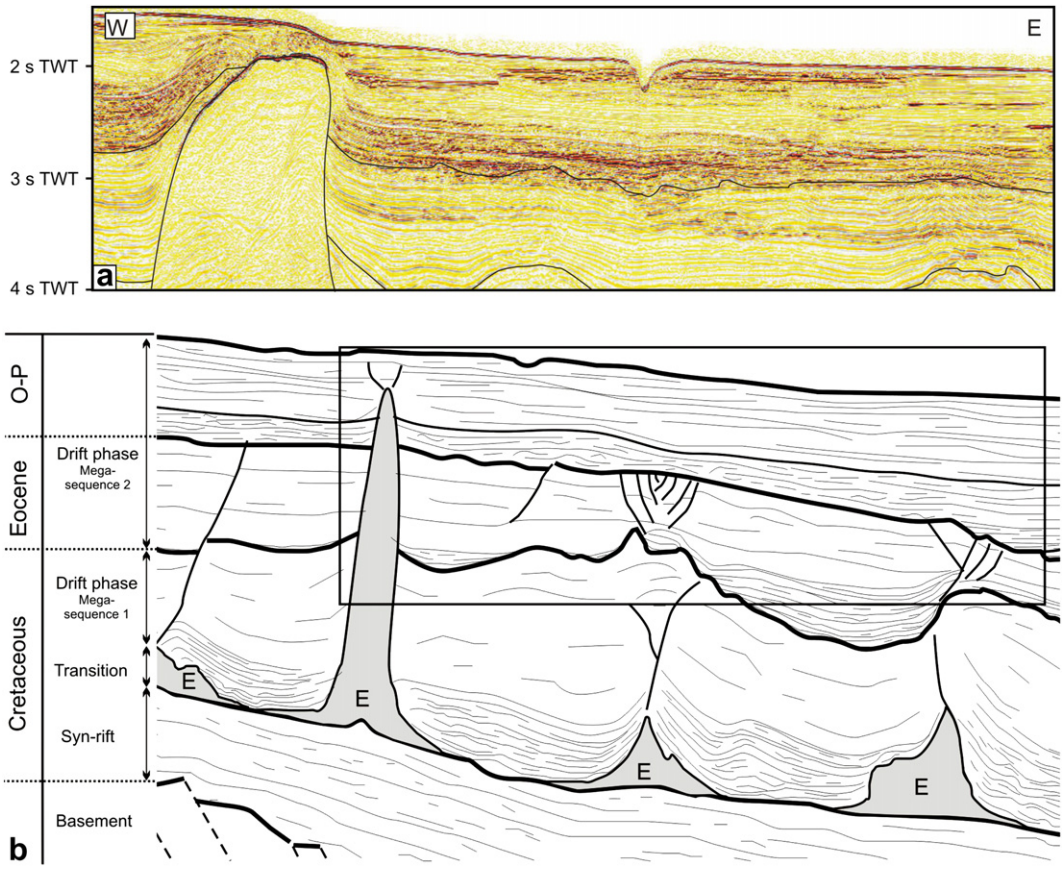

Fig. 2. (a) Seismic section across the 3D data in the BES-2 survey available for this study. (b) Schematic regional section across the Espirito Santo Basin (after Fiduk et al., 2004). Deformation of the evaporites (E) in major salt diapirs has been active since the Albian. N–S folding of the Cretaceous sequence and strata above results from early Cenozoic compression. O–P is Oligocene to Present day. A major unconformity (Top K) separates the Mesozoic and Cenozoic megasequences.

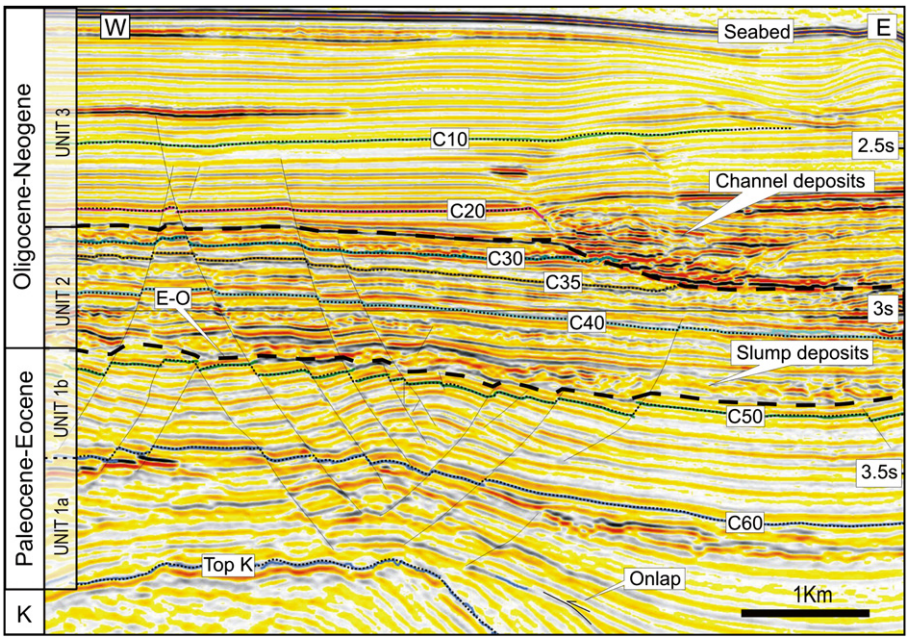

Fig. 3. 3D seismic section showing the main stratigraphic units above the Cretaceous (K) and key Cenozoic horizons. The erosional surface (E–O) at the base of Unit 2 is post middle Eocene to Oligocene in age.

4. Structural analysis and fault kinematics

4.1. General fault network

The faults in this dataset are localised in the vicinity of the recent salt diapirs and/or on the top of Cretaceous anticlines (Fig. 4). They are interpreted as typical crestal collapse structures (e.g. Bruce, 1973; McClay, 1990; Vendeville and Jackson, 1992) resulting from outer-arc stretching of the strata overlying anticlinal structures. Most faults only offset Unit 1 and do not offset the sediments above the E–O boundary at the base of Unit 2. The only faults that offset the stratigraphy above Unit 1b are located in the eastern part of the dataset and are interpreted as reactivated. The fault array affected by reactivation is characterised by a highly segmented pattern (Fig. 5).

The fault network was divided into straight segments to quantify fault strikes (Fig. 6). The rose plot displaying the strike of all faults shows two different populations (Fig. 6a). The faults located on the crest of the anticline are characterised by strike directions comprised between North and N050° with a mean value at N015°, which is very close to the direction of the axis of the anticline (N018°). The second population is more disparate with mean values striking between 120° and 130°. Rose diagrams illustrate that 43% of the faults terminate upwards at the E–O boundary and 57% are reactivated into Units 2 (Fig. 6c) and 3 (Fig. 6d). From the total length of reactivated fault segments, 79% strike in the direction of the main fault set (N to N050°). From the reactivated fault segments, c. 60% terminates downward at the top of the anticline, with c. 30% that probably detach on the limbs of the anticline (Fig. 7b). This observation indicates a close relationship between the detached faults and the occurrence of reactivation as shown by the 3D visualisation images (Fig. 7a,b) and the connection between locations of reactivated segments and isochrone 500 ms TWT of Horizon Top K (Fig. 5).

4.2. Geometry and kinematics of faults in Unit 1

The faults within Unit 1 form a graben system that tips out downwards on the crest of the anticline (Fig. 7a). Fault dimensions and displacement values decrease towards the centre of the graben system, suggesting that the faults nucleated progressively towards the centre of the crestal graben (McClay, 1990). The axial plane of the anticline strikes NE–SW and the fold axis plunges c. 2.3° toward the NE. This structure is interpreted as a semi-elliptical dome trending NE in the direction of Diapirs D1, D2 and D3 (Fig. 4). The graben system overlying this anticline in Unit 1 can be explained by elliptical doming with a small additional in plane extension when compared with the results of analogues models (Cloos, 1955, 1968; Withjack and Scheiner, 1982) or field analogue studies (Wendlandt et al., 1946; Parker and McDowell, 1951).

The kinematic history of faults offsetting Unit 1 is difficult to establish with certainty because the upper tip lines are truncated by the base of Unit 2. In addition, small growth faults with relatively regular and low displacement gradients can be very similar to faults that propagated blindly (Petersen et al., 1992; Baudon and Cartwright, 2008), further complicating the interpretation. The onset of faulting within Unit 1 occurred between the Early Cenozoic (formation of major anticlines) and the Late Eocene (E–O erosional surface). Subtle growth packages in close proximity to the fault planes in the upper part of Unit 1b (Fig. 8a) are associated with steep positive gradients on the throw profiles (i.e. profile 6 in Fig. 13). These indications of syn-sedimentary movement suggest that, regardless of the early kinematic evolution

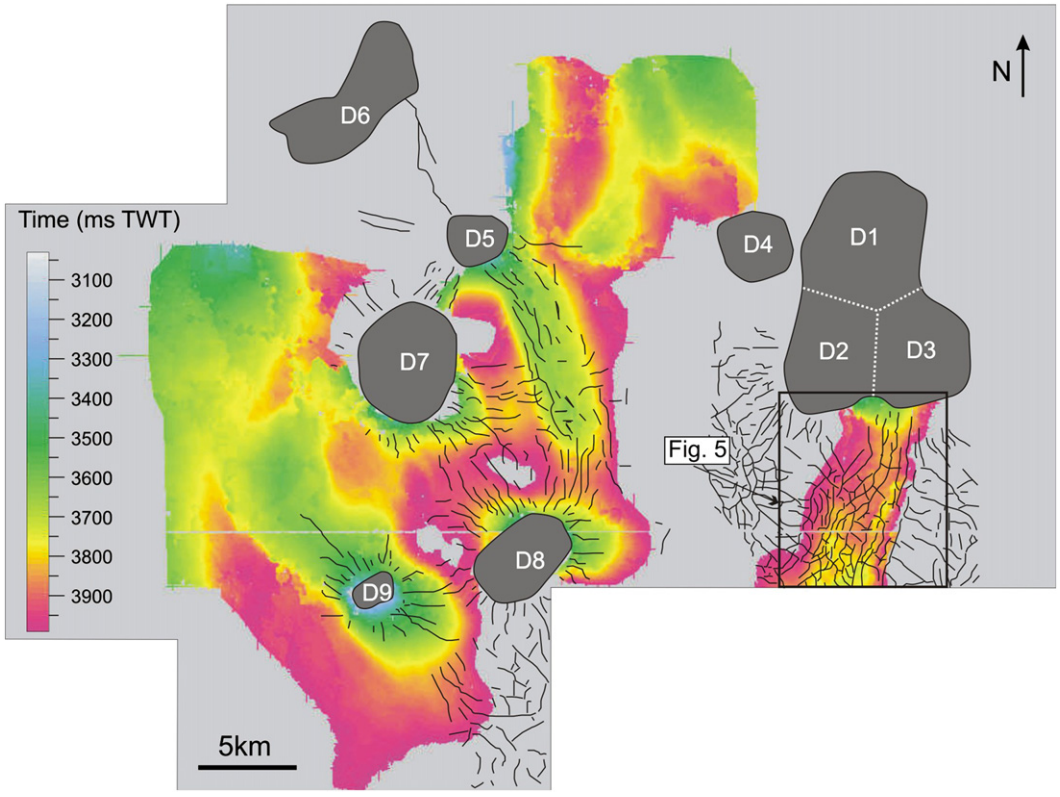

Fig. 4. Structural map of the Top Cretaceous Horizon in ms TWT from the 3D seismic survey. Dark grey rounded structures are the salt diapirs (D) piercing through the Cenozoic sequence. The fault network mapped on Horizon C50 is superimposed to the Top Cretaceous map.

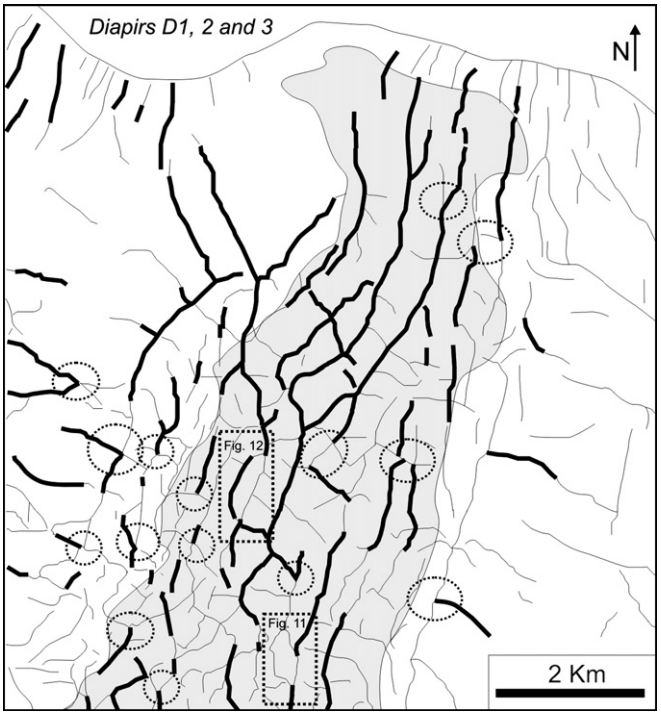

Fig. 5. Fault pattern based on the dip map of Horizon C50 situated in the upper part of Unit 1b. The figure shows non-reactivated faults (in thin lines) and reactivated fault segments (in thick lines). Dotted rectangles indicate the location of the examples of reactivation by upward propagation developed in Fig. 11 and reactivation by dip linkage analysed in Figs. 12 and 13. Typical examples of selective reactivation delimited by along-strike segmentation are highlighted with dotted circles. Grey area represents isochrone 500 ms TWT of Horizon Top K showing the relationships between the limbs of the anticlines and the occurrence of reactivated faults.

(growth faults or blind faults), these faults were active at the free surface in the Late Eocene. Faulting of Unit 1 occurred during a first period of deformation, which is attributed to Early Cenozoic–Late Eocene time.

4.3. Fault network in Units 2 and 3

Faults offsetting Units 2 and 3 predominantly strike between N and N050° (Fig. 5b). The fault planes are generally increasingly planar and steepen in the upper part. These portions of reactivated fault planes are interpreted to have propagated by blind propagation on the basis of the following criteria: (1) upper tip-lines plunge towards the lateral tips for individual faults, (2) faults terminating upward at different stratigraphic levels (Childs et al., 2003; Baudon and Cartwright, 2008), (3) absence of stratigraphic thickening in the hanging wall or evidence of scarp, and (4) upper-tip folding in a monocline style as expected ahead of propagating blind faults (e.g. Gawthorpe et al., 1997). In addition to these observations, the characteristics of throw distribution on these upper portions of reactivated faults are typical for the range of upper-tip gradients of blind faults (Fig. 10b). All these criteria strongly suggest that the faults grew by blind propagation above the E–O boundary, so that sediments of Unit 2 and most of Unit 3 were deposited before the second period of deformation.

The kinematic history proposed for the crestal-collapse faults can be summarised in a three-step model, illustrating two distinct phases of faulting separated by a period of quiescence (Fig. 9).

5. Characteristics of reactivation

5.1. Throw distribution analysis on faults

Representative vertical throw-distribution plots for the faults located in the reactivated area were grouped into two main populations. The first group includes profiles of non-reactivated faults that terminate upward at the E–O boundary (Fig. 10a) and the second group contains reactivated faults terminating within Units 2 or 3 (Fig. 10b).

5.1.1. Non-reactivated eroded faults

The vertical throw distribution on faults that only offset Unit 1 are truncated in the upper portion where throw values of the shallowest measurable offset horizon range from c. 5 to 20 m

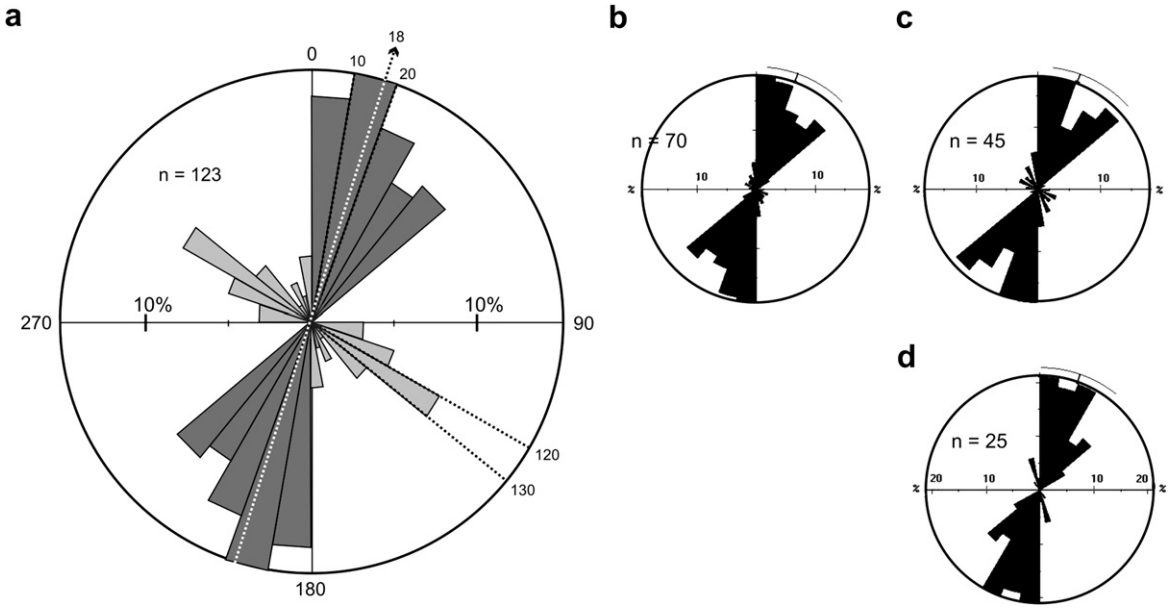

Fig. 6. Rose diagrams of fault network located in the SE part of the survey. The fault network was divided into small straight segments. Vertical and horizontal axes show percentage of fault segments (based on total fault length). *n* indicates the number of fault segments measured. (a) Rose plot representing the strike of all faults. White dashed line indicates the strike of the axial plane of the anticline. (b) Rose plot for reactivated faults terminating in Units 2 and 3. (c) Reactivated faults terminating in Unit 2 only. (d) Reactivated faults terminating in Unit 3 only.

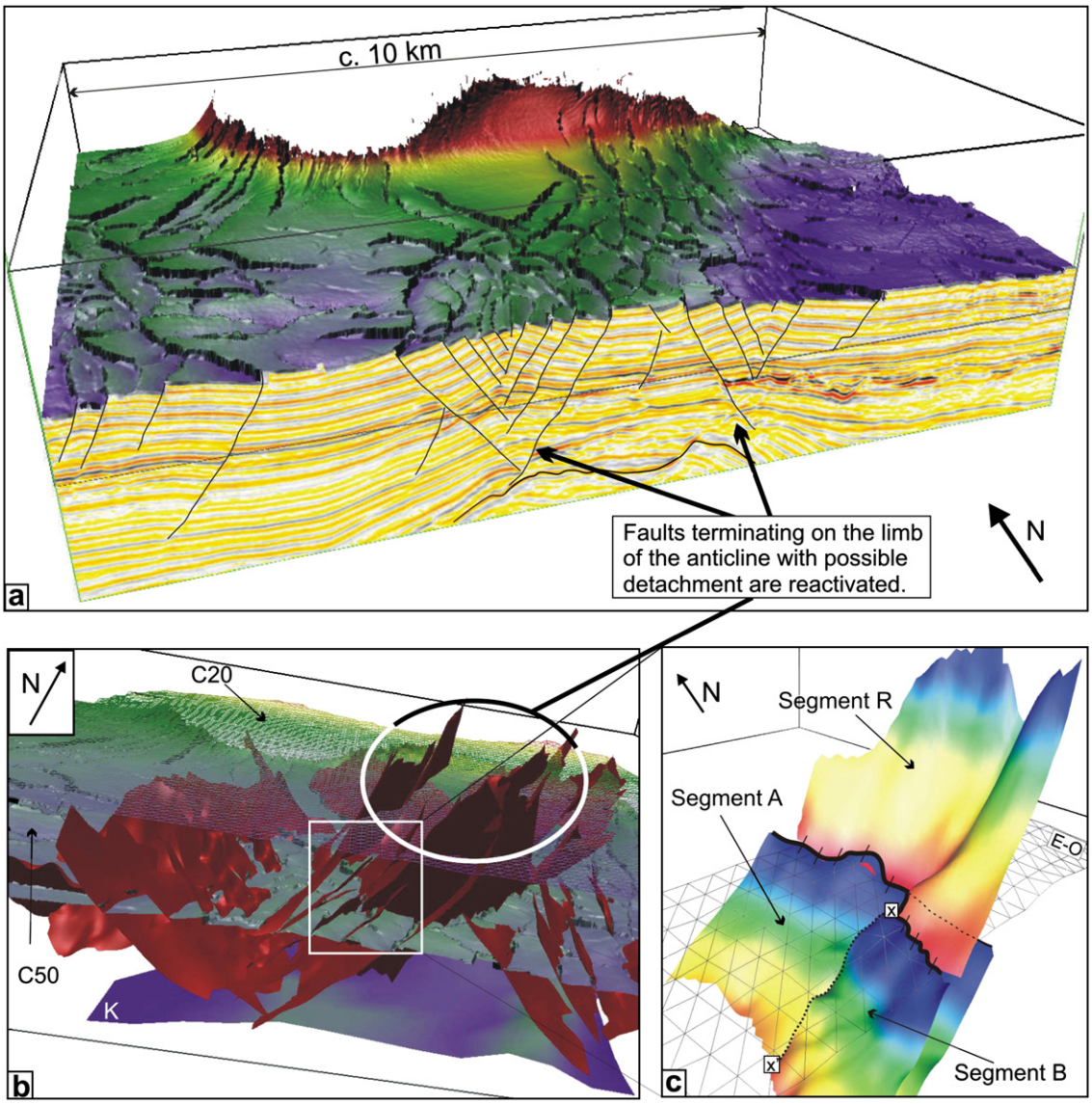

Fig. 7. Geoviz visualisations showing the fault network with key surfaces. (a) 3D block diagram showing the faults in seismic section with a map of Horizon C50. (b) 3D visualisation of the fault planes (in red colour) organised in a crestal collapse graben. Most reactivated faults terminate on the limbs of the Cretaceous anticlines (K). Key surfaces are Horizon C50 situated at the top of Unit 1b and Horizon C20 at the base of Unit 3. (c) Close-up of an example of reactivation by dip linkage (details in Figs. 12 and 13). Segment B intersects Segment A through a dip-parallel branch line (*x*–*x*′). Segment R initiated individually above the Eocene–Oligocene boundary (E–O) and propagated downward to hard link with Segment A towards the NE and switches to link with Segment B towards the SW.

(Fig. 10a). These correspond to fault segments eroded by the slump horizons identified on seismic sections (Fig. 8b). The vertical throw-distribution plots are mostly characterised by M-type or C-type throw-profiles. The intervals with maximum throw values (up to c. 25 m) are located dominantly within Unit 1b, between Horizons C50 and C60. Maximum throw-values for faults that tip out downwards without detachment are located within Unit 1b whereas faults that detach generally exhibit throw maxima in Unit 1a.

5.1.2. Reactivated faults

Most faults that terminate upward in Units 2 and 3, and are hence interpreted as reactivated, exhibit stepped vertical throw-profiles, which can be typically separated into two parts (Fig. 10b). The lower part has a similar shape to the *T*–*z* plot for non-reactivated faults. Although the shapes are comparable, the magnitude of the throw values is systematically greater for the reactivated faults compared to the non-reactivated faults with average maximum throw values of c. 45 m. The central and upper parts of the *T*–*z* profiles (i.e. above the E–O boundary to the upper tip) are generally characterised by almost constant positive throw gradients per individual faults, whose values range from 0.01 to 0.07 (e.g. profiles 6, 7 and 8). Less commonly, there is a change of throw gradient within Unit 2 and Unit 3 (e.g. profile 5).

All reactivated faults exhibit an abrupt step in throw profiles at the E–O boundary. These steps are interpreted as characteristic of reactivation, and are not attributed to lithological effects during fault propagation through mechanical barriers (e.g. Gross et al., 1997; Wilkins and Gross, 2002). Contrasts in acoustic impedance of the sediments above and beneath this boundary are not sufficient to infer a major change in the mechanical properties. The reduction in fault throw above the E–O boundary is too large to be attributed only to a weak layer. Also, increase of throw gradients just beneath the boundary (i.e. profile 9) is attributed to the growth packages at the remnant upper tip regions of faults truncated at this boundary, indicating that the

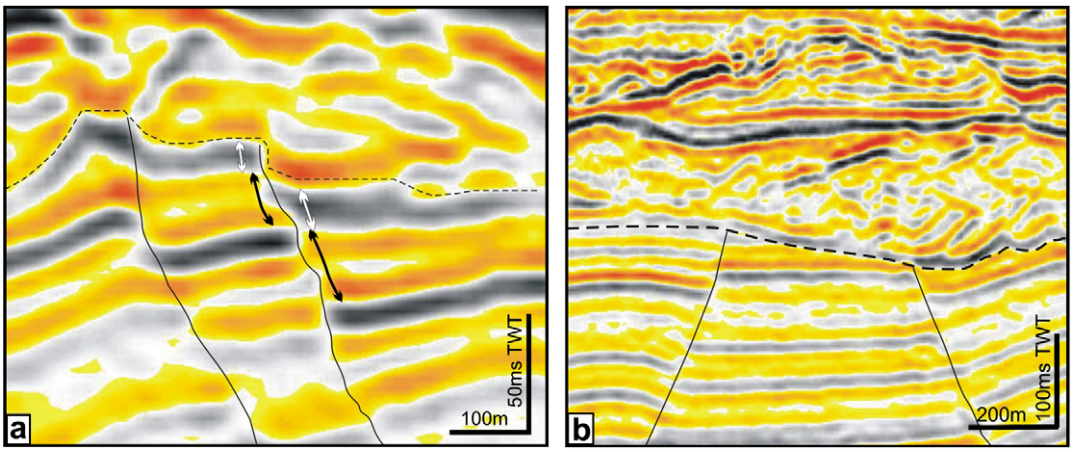

Fig. 8. (a) Seismic sections showing growth packages (shown by the arrows) situated at the top of Unit 1. (b) Seismic section showing erosional truncation surface (in dashed line) at the base of the slump interval.

majority of these faults were active in a synsedimentary mode before erosion by the slump unit and deposition of Units 2 and 3. These faults cannot therefore be treated as exclusively blind faults as is required for a purely lithological explanation of the stepped profiles.

5.2. Modes of reactivation

Two distinct modes of reactivation are recognised from a combination of 3D fault-plane mapping and throw analysis. These two modes are referred to here as: (1) 'upward propagation', where reactivation is by dominantly upward propagation of selected segments of existing faults, and (2) reactivation by dip linkage, where a new fault nucleates in the cover sediments above a pre-existing fault (the parent fault). A reactivated and enlarged fault may also form by a combination of the two modes.

5.2.1. Reactivation by upward propagation

The vast majority of the reactivated faults grew by upward propagation from the parent fault and many only had specific portions of the parent fault surface reactivated (Figs. 5 and 11). For the example illustrated in Fig. 11, the central region of the parent fault was not reactivated. This central portion is delimited by branch lines with intersecting faults, and a close spatial association exists between the original segmentation of the parent fault and the subsequent selective reactivation.

The upward propagation mode of reactivation can be recognised in the throw distribution on the reactivated fault (Fig. 11b). The upper tip line varies laterally in position from 2400 ms TWT at the lateral regions to 3000 ms TWT in the central portion of the fault. The basal tip line is located at c. 3800 ms TWT at the SSW and the central regions (lines 1–6) and terminates at progressively shallower levels up to 3550 ms TWT at the NNE lateral tip. The seismic data show the fault detaching on the limb of the underlying anticline between lines 1 and 6 whereas in contrast the lower tip line abuts against an antithetic fault between lines 7 and 11. Regions of maximum throw values are located between 3000 and 3800 ms TWT. More specifically, the contours are centred on two maxima situated between 3700 and 3800 ms TWT on those portions of the fault plane that detach at the base. Above the E–O boundary the contours are more widely spaced and sub-horizontal with no sign of perturbation or local maxima.

T–z plots for the central portion of the fault plane (*T–z* plots 4, 5 and 6) are characterised by typical profiles of non-reactivated faults (Fig. 10a). Throw maxima are located in the lower part of the profile between C60 and Top Cretaceous horizons as expected for detaching faults. The *T–z* plots obtained for the portions of faults that are interpreted as reactivated (*T–z* plots 1, 2, 3, 7, 8, 9, 10 and 11) exhibit typical stepped profiles with a major break in throw gradients corresponding with the E–O boundary. Upper parts of the profiles overlying the E–O boundary are generally characterised by a constant positive throw gradient between c. 0.01 and 0.06 (such as *T–z* plots 7, 9 and 10). Alternatively, some profiles exhibit a near zero gradient between the E–O boundary and Horizon C30 (such as *T–z* plots 1, 2 and 11). However, C-type profiles are absent in the upper parts of these *T–z* plots or lack significant irregularities in the throw gradients.

5.2.2. Reactivation by dip linkage

Dip linkage is a much less common mode of reactivation (c. 5% of reactivated faults in this dataset), but is nonetheless interesting and with potentially wider implications for reactivation in fault systems where strong mechanical layer anisotropy favours localisation of new faults in different mechanical 'tiers'. An example of reactivation by dip linkage is presented in this section (Figs. 7c, 12 and 13). Segments A and B are pre-existing faults offsetting Unit 1 and Segment R is a fault that initiated individually within Units 2 or 3 above Segments A and B and strikes in a similar direction (Fig. 7c). A map view of Horizon C50 with 3 seismic sections taken along strike illustrates the spatial relationship between these faults (Fig. 12a). In the northern part of the fault, Segment A is reactivated by dip linkage with Segment R (Fig. 12b). In the region of northern branch line (x–x'), Segment R is separated from Segment A by a relay zone at the E–O boundary (Fig. 12c). Further south, Segment R switches toward the west to link with Segment B, which is reactivated, leaving Segment A truncated at the E–O boundary (Fig. 12d). At the southern branch line (y–y') between Segments A and B, Segment R switches back to reactivate a dip link to Segment A. One conditions for facilitating reactivation by dip linkage is the similarity between the dips and strikes of the segments nucleating in the upper units and the parental segments beneath. In addition to this similarity, segmentation of the pre-existing network is clearly controlling the location for selective reactivation (Fig. 5).

The throw distribution of the reactivated fault provides additional evidence for the dip-linkage interpretation (Fig. 13b). Toward the NNE and the SSW the upper tip-line of the fault terminates between 2300 and 2400 ms TWT, but is deeper at c. 3000 ms TWT in the central portion where Segment A is not reactivated. Two principal throw maxima are located between 3000 and 3400 ms TWT. The throw contours above the E–O boundary are irregular but crudely centred on small individual zones of maximum throw values such as between 2800 and

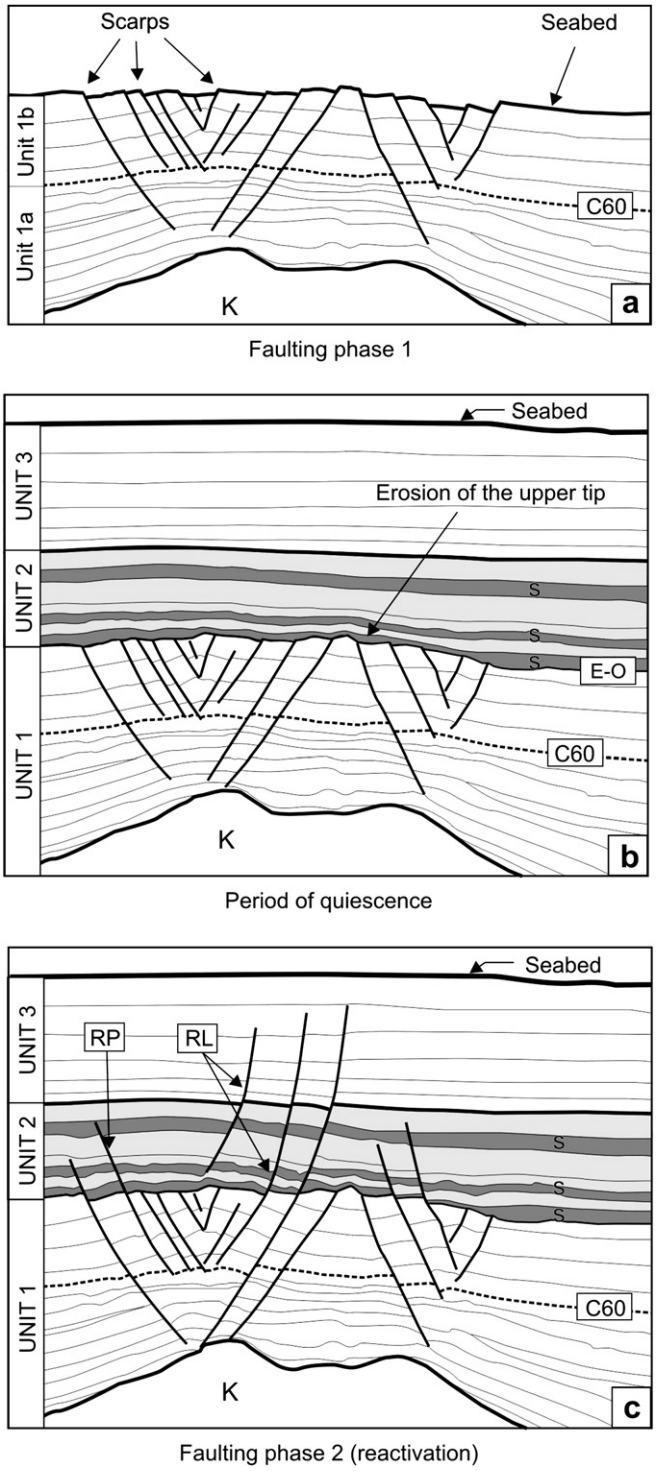

Fig. 9. A three-step evolutionary model for the crestal graben faults. (a) First phase of faulting occurred between the early Cenozoic (time of formation of major anticlines) and the late Eocene (time of deposition of the sediments in the upper part of Unit 1b). Most of the uplift of the Cretaceous sequence (K) was contemporaneous with the deposition of sediments that compose Unit 1a. The faults offsetting Unit 1 were active at the deposition of the upper part of Unit 1b. (b) Period of quiescence during deposition of Units 2 and 3. (c) Phase of faulting 2 by blind propagation of post-sedimentary faults resulting in the reactivation of faults situated in Unit 1 by upward post-sedimentary propagation (RP) into Units 2 and 3 or reactivation by linkage (RL) of a fault that initiated in Units 2 and 3 and propagated downwards to link with faults in Unit 1. Dark shaded areas (s) represent the slump deposit intervals.

3000 ms TWT in the vicinity of line 3. This throw maximum is separated from the lower part of the fault plane by a horizontal zone of throw minima located in the vicinity of the E–O boundary at c. 3000 ms TWT.

Vertical throw distribution plots also show subtle details of reactivation by dip linkage (Fig. 13c). *T–z* plots obtained on Fault A where it overlaps with Segment B (*T–z* plot 4) is characterised by a profile typical of non-reactivated faults (Fig. 10a). Elsewhere, throw profiles have two parts separated by a sharp change in throw values and gradients as is expected for reactivated faults (Fig. 10b). The upper part of these profiles above the E–O unconformity does not always have single positive gradients. *T–z* plots 1, 2, 3, 6 and 7 are characterised by throw profiles resembling C-type patterns (cf. Baudon and Cartwright, 2008) between the upper-tip point and Horizon C20. Throw profiles 3 and 5 exhibit a C-type vertical throw-distribution plot between C30 and the E–O boundary. This difference is interpreted as being the consequence of reactivation by dip linkage of individual Segment R. The zone of linkage between two originally individual segments that are hard linked is recognisable by a zone of throw minima and steepening of the throw gradients (e.g. Peacock and Sanderson, 1994; Cartwright et al., 1995). This segment initiated within the upper part and propagated downward to link with the upper tip line of pre-existing Fault A.

Faults that are reactivated by the dip-linkage process are characterised by stepped profiles with a major break in throw gradients and possible zones of separated C-shape profiles above the E–O boundary. This type of reactivation is recognisable by throw maxima in the upper part of the fault plane separated from the pre-existing parts by throw minima.

6. Discussion

6.1. Modes of reactivation

Reactivated structures have previously been described as growing by further propagation of the pre-existing structure after a significant period of quiescence (e.g. Holdsworth et al., 1997; Nicol et al., 2005). The classical model for reactivation is described as upward propagation from pre-existing structure as faults are generally generated at depth and grow upward (Richard and Krantz, 1991). This study has identified two distinct modes of reactivation for the crestal extensional faults, upward propagation and dip linkage. Both modes of reactivation are recognised by typical stepped profiles with a major break in throw gradients corresponding to the E–O boundary. Subtle differences in the throw distribution provide insights into the recognition of either mode. Upward propagation is characterised by profiles exhibiting a regular decrease in throw values and gradients up to the upper tip point (Fig. 11), whereas reactivation by dip linkage can be identified by throw maxima in the upper part of the fault plane separated from the pre-existing parts by throw minima (Fig. 13). Further growth of the two hard-linked segments after reactivation might attenuate the throw variations and obscure the differentiation of these two types of reactivation.

6.2. Preferential reactivation

6.2.1. Direction of reactivation extension

The probability of reactivation is directly related to the orientation of the fault planes relative to the principal stresses and their ability to accommodate the imposed strains (White et al., 1986; Richard and Krantz, 1991), as well as difference in friction coefficients and cohesion (Sibson, 1985).

Evaluating the direction of extension during reactivation is difficult. However, the faults interpreted as reactivated from the 3D seismic data mostly strike in a NNE–SSW direction, especially the

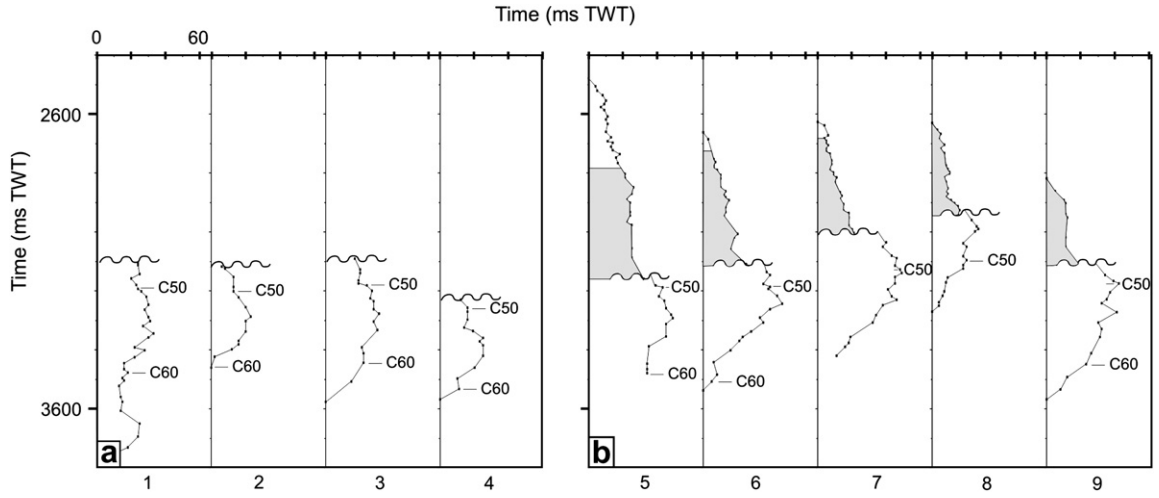

Fig. 10. Vertical throw–distribution plots. Each *T*–*z* plot represents the throw values plotted against the time in ms TWT. (a) Faults that are eroded by the E O surface and are not reactivated are characterised by truncated throw profiles. (b) *T*–*z* plots for reactivated faults. C50 and C60 are key horizons, the wavy line indicates the location of E–O erosional surface and Unit 2 is represented by the shaded area.

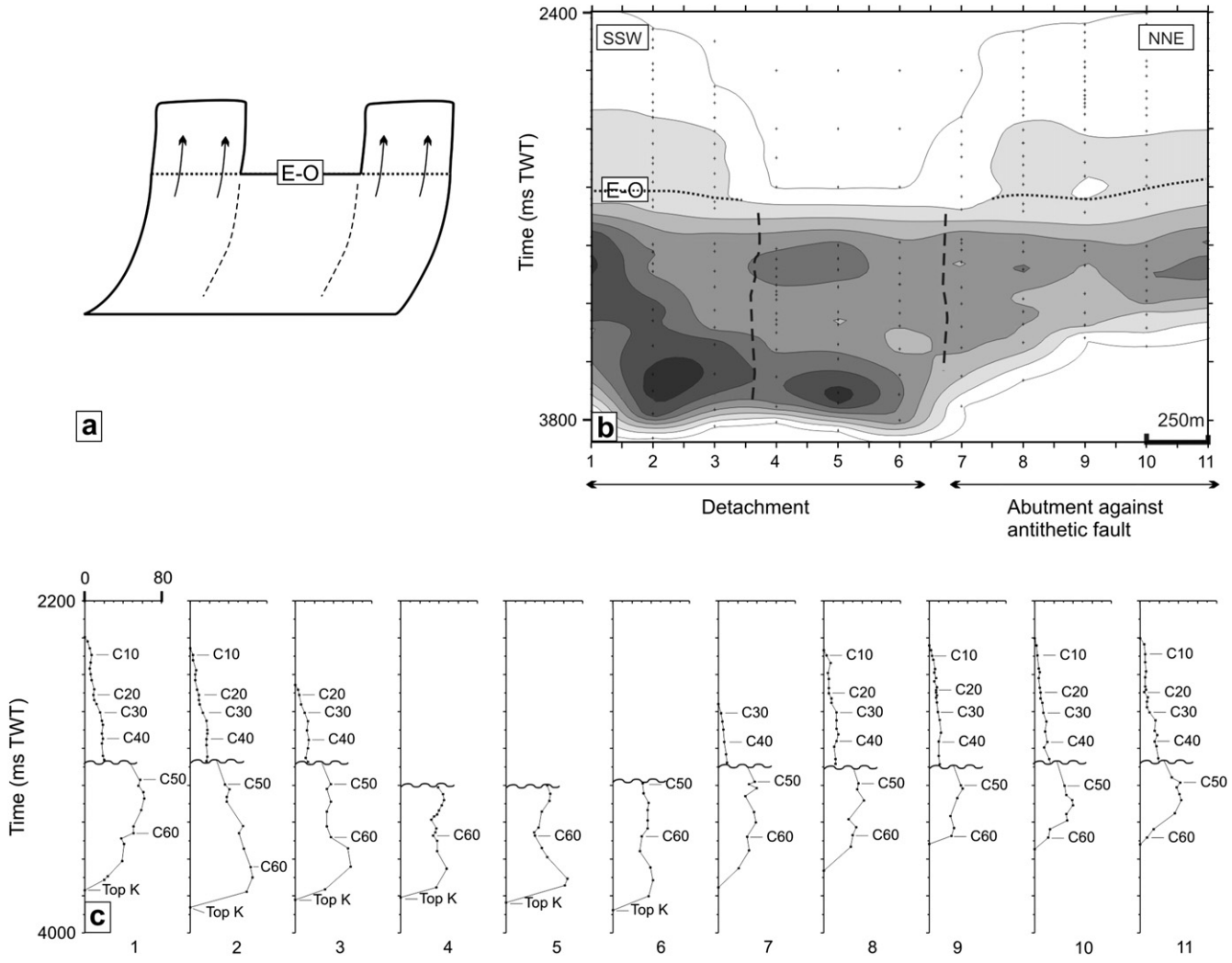

Fig. 11. (a) Schematic illustration of the 3D geometry of a typical example of a fault that reactivated by upward propagation (indicated by the arrows). The central portion that is not reactivated is delimited by dip-parallel branch lines of interacting faults (dashed lines). (b) Throw contour plot showing lines of equal throw value spaced every 10 ms TWT and up to 70 ms TWT (dark colour). Dotted lines indicate the areas of reactivation. (c) Vertical throw distribution plot for a reactivated fault by upward propagation. Each *T*–*z* plot shows the throw values (*T*) up to 80–ms TWT against the time in ms TWT. Wavy lines represent the E–O boundary.

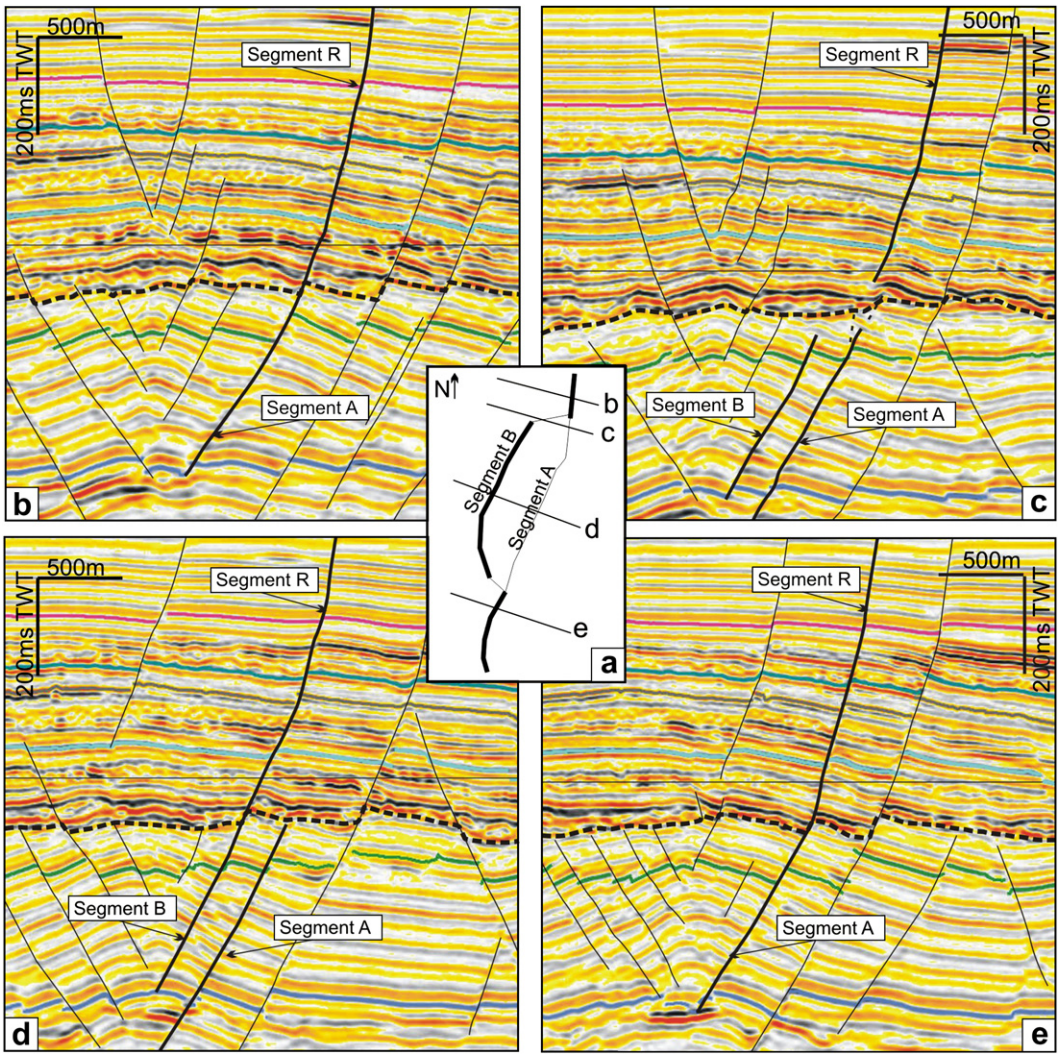

Fig. 12. Example of reactivation by dip linkage. (a) Map view of fault geometry with location of the seismic-sections shown in (b)–(e). Location of this fault is indicated by the rectangle in Fig. 5a–d. Seismic sections along strike of the structure. Dashed line is the E–O boundary: (b) Segment A is reactivated, (c) Segment R is separated from the lower-tier faults, (d) Segment R dip link with Segment B, Segment A is not reactivated anymore, (e) Segment R switches back to reactivate Segment A.

faults that tip out in Unit 3 (Fig. 6). The dominant trend of reactivated faults suggests that the orientation of the pre-existing fault planes with respect to the direction of the principal stress axis characterising the second phase of deformation is an important factor influencing preferential reactivation. In addition to this relationship, comparison of the fault network with analogue modelling and field studies suggests that this geometry is due to a WNW–ESE extension, which is concordant with the orientation of the Cretaceous anticlinal axis (N018°). This direction also corresponds to the orientation of the second and smaller population of faults striking between N120° and N130°.

This interpretation suggests that the selection for reactivation is strongly influenced by the orientation of the faults with respect to the principal stress axes of the phase of deformation resulting in reactivation. However, no quantitative conclusion can be drawn in the absence of further information on the direction of the second extensional phase.

6.2.2. Selective reactivation influenced by segmentation

The crestal-collapse faults from the Espirito Santo Basin are interpreted to be reactivated depending on their orientation. However, it is also observed that faults do not always reactivate along the entirety of their length. Particular portions or segments of faults are preferentially reactivated although several non-reactivated segments strike in a similar direction as the reactivated segments (Fig. 5). Therefore, the reactivation must be influenced by factors other than the faults orientation.

This study proposes that preferential reactivation is also related to fault segmentation or connectivity as previously suggested (Kelly et al., 1999). The portions of major faults that are reactivated are often delimited by intersections with other fault segments (Fig. 5). The horizontal limits of reactivation often correspond to overlapping zones with other interacting faults and zones of linkages through the branch lines on the fault planes (Figs. 5, 11 and 13). It must be noted that 5–10% of reactivated portions are not delimited by branch line or interaction with another structure that is observable at seismic scale (Fig. 5).

6.2.3. Influence of the dimensions of faults and basal tip geometry on selective reactivation

Preferential reactivation has been attributed to larger faults partly due to the weaker friction associated with their smooth fault plane (Scott et al., 1994) and an abundance of fluid circulation in large fault networks (Kelly et al., 1999). It was suggested that in some cases smaller faults offsetting the cover do not reactivate as opposed to some larger basement faults, which are not factors for

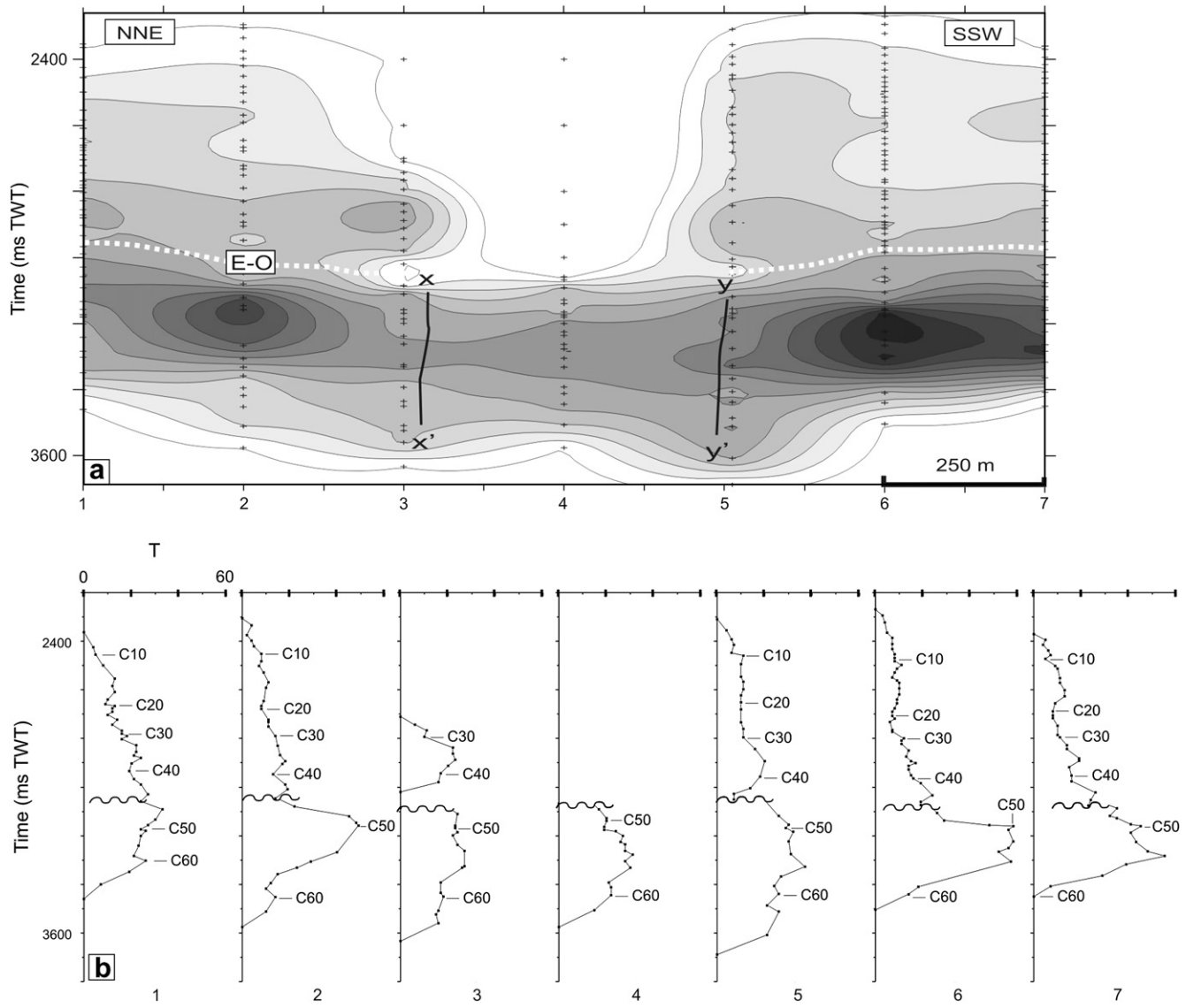

Fig. 13. (a) Schematic illustration of the 3D geometry and interaction between Segments A, B and R. Segment R hard linked with Segment A by downward propagation and re-activated it on most of the strike length except in the centre of the fault plane where Segment R reactivated Segment B. Dotted lines indicate the branch lines of dip linkage and arrows show the direction of propagation. (b) Throw contour plot showing lines of equal value up to 60 ms TWT (spacing is 10 ms TWT) on the main fault plane (Segment A) and the reactivated upper tip (Segment R). Branch lines of dip linkage between Segments A and R are indicated by dotted white lines. (c) Vertical throw–distribution plots for Fault A. Each *T*–*z* plot represents the throw values (*T*) up to 60 ms TWT plotted against time.

these faults in the Espirito Santo Basin because they are all small and offset the cover.

The magnitude of the throw values is greater for the reactivated faults compared to the non-reactivated faults (Fig. 10). The question remains whether these portions that were reactivated because of their great throw values are representative of mechanically more efficient slip locations or if they gained great throw values only through reactivation. Comparison of reactivated with non-reactivated portions of faults illustrating reactivation by upward propagation (Fig. 11) and dip linkage (Fig. 13) provides insight into this issue. In the case of upward propagation, the SSW reactivated segments exhibit larger throw values than either the non-reactivated central part or the NNE reactivated segment. Interestingly, the SSW reactivated segment detaches on the limb of the anticline. This observation perhaps suggests that other controls such as the geometry of the basal tip region affect the selection of reactivated portions. In the dip linkage example, Segment R linked to Segment B although overlapping Segment A is characterised by greater throw values. In this case, the orientation of the upper-tier fault with respect to the faults located in Unit 1 is clearly a dominant factor on selective reactivation rather than the dimension or maximum throw values.

The possibility that the occurrence of reactivated fault segments is linked to the basal-tip geometry with respect to the anticline is further supported by more general mapped relationships in the study area. Of the total cumulative length of reactivated fault segments, along 60% of this length, the segments are observed to terminate downward into the flanks of the anticline and detach on the limbs of the anticline (Figs. 7b and 8). One interesting observation regarding the basal-tip geometry is that faults that tip out downward without detachment exhibit throw maxima within Unit 1b whereas faults that detach on the anticline flanks generally exhibit throw maxima in Unit 1a (Fig. 13). Detached faults have larger throw values than non-detached faults, so the characteristics of fault basal-tip regarding the anticline are correlated with the throw magnitude. It is therefore proposed that the basal tip

geometry and location in relationship to the crest and limbs of the anticlines influence the selection of particular faults for reactivation.

6.3. Implications

As previously suggested in earlier papers on fault growth (e.g. Walsh et al., 2002; Vetel et al., 2005), a reactivated structure can exhibit an abnormally low displacement-to-length ratio (D/L). The length of faults is generally established during the phase of faulting that created the pre-existing faults. When the faults are reactivated, a disproportionate increase of maximum displacement relative to length shifts the growth path in a plot of displacement versus length to a path with higher D/L ratio. In the case of the Espirito Santo basin faults, the length was established during faulting phase 1. The reactivated faults resulting from faulting phase 2 accumulated twice the amount of displacement whist maintaining near constant fault trace length. It is therefore necessary to consider reactivation as an important factor for scatter in D/L ratio as these scaling relationships are used to promote several fault growth models (e.g. Walsh and Watterson, 1988; Cowie and Scholz, 1992a; Cartwright et al., 1995). Models of fault evolution of this type also provide insights into the timing of fault activity which has a direct application to hydrocarbon migration and sealing of faults in petroleum reservoirs (McClay, 1990). For example, accurate timing of any reactivation phases with reference to constraints on the filling of hydrocarbon traps would be critical for an evaluation of seal risk (Cartwright et al., 2007). Traps are much more likely to leak during periods of fault reactivation than during periods when the faults are inactive, all other parameters of seal integrity being the same (Hooper, 1991; Gartrell et al., 2002; Cartwright et al., 2007). A further understanding of reactivation processes will greatly improve petroleum prediction of seal integrity, trap geometry and fluid circulation or migration. The different modes of reactivation discussed here may also be relevant for consideration of reactivation potential of seismogenic basement faults in that structural context and the geometry of deeper detachments may be a significant factor in priming a given segment for later reactivation (Sibson, 1981; Hickman et al., 1995).

7. Conclusions

This paper investigated the kinematics of small crestal collapse faults offsetting Cenozoic clastic sediments that overlie Cretaceous anticlines using high quality 3D seismic data from offshore Brazil. Geometrical, kinematic and stratigraphic evidence were presented to demonstrate the occurrence of reactivated faults in the study area. (1) A large percentage of the fault network terminates upward at the E–O erosional surface located at the base of Unit 2. (2) The faults were active at the free surface at the time of deposition of the sediments that form the upper part of Unit 1b. (3) Fault segments offsetting Units 2 and 3 grew entirely by blind propagation. The second phase of faulting is post-sedimentary and therefore implies a period of quiescence while deposition of Units 2 and 3. (4) An abrupt step in the vertical throw distribution (T–z plots) marks the zone of newly propagating portions of faults.

Two different modes of reactivation are recognised. The main mode is a classical reactivation by upward propagation of pre-existing structures. The second mode, which is termed reactivation by dip linkage, involves the propagation of an individual fault initiated within the upper Units 2 and 3 during the second phase of faulting. Further propagation of these faults result in hard linkage in the dip direction with pre-existing faults. Throw profiles and contour plots exhibit a regular decrease in throw values and gradients up to the upper tip for reactivated faults by upward propagation. Throw minima separate the upper parts from the pre-existing fault in the case of reactivation by dip linkage. For both modes, reactivation processes are selective and only occur on portions of some faults. The factors that control or influence the preferential reactivation of some portions amongst others are: (i) preferential orientation of the pre-existing faults at 90–110° relative to the estimated principal stresses resulting in faulting phase 1, (ii) segmentation of the pre-existing network, (iii) maximum dimensions and throw values of pre-existing faults, and (iv) basal tip-line geometry associated with a detachment.

Acknowledgements

We wish to thank the Compagnie Générale de Géophysique for supplying the seismic data and permission to publish this work. Schlumberger Ltd is acknowledged for providing Geoquest seismic interpretation software. This paper has benefited from discussions with Richard Davies, Richard Lisle and Simon Higgins. Two anonymous reviewers and Editor William M Dunne are thanked for thoughtful and constructive reviews which greatly improved the manuscript.

References

Austin, J.A., Uchupi, E., 1982. Continental–oceanic crustal transition off southwest Africa. American Association of Petroleum Geologists Bulletin 66 (9), 1328–1347.

Baudon, C., Cartwright, J.A., 2008. 3D seismic characterisation of an array of blind normal faults in the Levant Basin, Eastern Mediterranean. Journal of Structural Geology 30 (6), 746–760.

Bellahsen, N., Daniel, J.M., 2005. Fault reactivation control on normal fault growth: an experimental study. Journal of Structural Geology 27 (4), 769–780.

Blair, T.C., Bilodeau, W.L., 1988. Development of tectonic cyclothems in rift, pull-apart, and foreland basins: sedimentary response to episodic tectonism. Geology 16 (6), 517–520.

Brewer, J.A., Smythe, D.K., 1984. MOIST and the continuity of crustal reflector geometry along the Caledonian–Appalachian orogen. Journal of the Geological Society 141, 105–120.

Bruce, C.H., 1973. Pressured shale and related sediment deformation: mechanism for development of regional contemporaneous faults. American Association of Petroleum Geologists Bulletin 57 (5), 878–886.

Butler, R.W.H., Holdsworth, R.E., Lloyd, G.E., 1997. The role of basement reactivation in continental deformation. Journal of the Geological Society London 154 (1), 69–71.

Cartwright, J.A., Trudgill, B.D., Mansfield, C.S., 1995. Fault growth by segment linkage: an explanation for scatter in maximum displacement and trace length data from the Canyonlands Grabens of SE Utah. Journal of Structural Geology 17 (9), 1319–1326.

Cartwright, J.A., Bouroullec, R., James, D., Johnson, H.D., 1998. Polycyclic motion history of some Gulf Coast growth faults from high-resolution displacement analysis. Geology 26 (9), 819–822.

Cartwright, J., Huuse, M., Aplin, A., 2007. Seal bypass systems. American Association of Petroleum Geologists Bulletin 91 (8), 1141–1166.

Chang, H.K., Kowsmann, R.O., Figueiredo, A.M.F., Bender, A.A., 1992. Tectonics and stratigraphy of the East Brazil Rift system: an overview. Tectonophysics 213 (1-2), 97–138.

Childs, C., Nicol, A., Walsh, J.J., Watterson, J., 2003. The growth and propagation of synsedimentary faults. Journal of Structural Geology 25, 633–648.

Cloos, E., 1955. Experimental analysis of fracture patterns. Geological Society of America Bulletin 66 (3), 241–256.

Cloos, E., 1968. Experimental analysis of Gulf Coast fracture patterns. American Association of Petroleum Geologists Bulletin 52 (3), 420–444.

Cowie, P.A., Scholz, C.H., 1992a. Displacement-length scaling relationship for faults: data synthesis and discussion. Journal of Structural Geology 14 (10), 1149–1156.

Cowie, P.A., Scholz, C.H., 1992b. Physical explanation for the displacement–length relationship of faults using a post-yield fracture mechanics model. Journal of Structural Geology 14 (10), 1133–1148.

Demercian, S., Szatmari, P., Cobbold, P.R., 1993. Style and pattern of salt diapirs due to thin-skinned gravitational gliding, Campos and Santos basins, offshore Brazil. Tectonophysics 228 (3-4), 393–433.

Enfield, M.A., Coward, M.P., 1987. The structure of the West Orkney Basin, northern Scotland. Journal of the Geological Society 144, 871–884.

Fiduk, J.C., Brush, E.R., Anderson, L.E., Gibbs, P.B., Rowan, M.G., 2004. Salt deformation, magmatism, and hydrocarbon prospectivity in the Espirito Santo Basin, offshore Brazil. In: Post, P.J., Olson, D.L., Lyons, K.T., Palmes, S.L., Harison, P.F., Rosen, N.C. (Eds.), Salt–Sediment Interactions and Hydrocarbon Prospectivity: Concepts, Applications, and Case Studies for the 21st Century. GCSSEPM 24th Annual Research Conference, pp. 370–392.

Gartrell, A., Lils, M., Underschultz, J., 2002. Controls on the trap integrity of the Skua oil field, Timor Sea. In: Keep, M., Moss, S.J. (Eds.), The Sedimentary Basins of

Western Australia 3: Proceedings of the Petroleum Exploration Society of Australia Symposium, pp. 389–407. Perth.
Gawthorpe, R.L., Sharp, I., Underhill, J.R., Gupta, S., 1997. Linked sequence stratigraphic and structural evolution of propagating normal faults. Geology 25 (9), 795–798.
Gross, M.R., Gutierrez-Alonso, G., Bai, T., Wacker, M.A., Collinsworth, K.B., Behl, R.J., 1997. Influence of mechanical stratigraphy and kinematics on fault scaling relations. Journal of Structural Geology 19 (2), 171–183.
Hickman, S., Sibson, R., Bruhn, R., 1995. Introduction to special section: mechanical involvement of fluids in faulting. Journal of Geophysical Research 100, 12. 831-12 840.
Holdsworth, R.E., Butler, C.A., Roberts, A.M., 1997. The recognition of reactivation during continental deformation. Journal of the Geological Society London 154, 73–78.
Hooper, E.C.D., 1991. Fluid migration along growth faults in compacting sediments. Journal of Petroleum Geology 14 (2), 161–180.
Jackson, J.A., 1980. Reactivation of basement faults and crustal shortening in orogenic belts. Nature 283 (5745), 343–346.
Kelly, P.G., Peacock, D.C.P., Sanderson, D.J., McGurk, A.C., 1999. Selective reverse-reactivation of normal faults, and deformation around reverse-reactivated faults in the Mesozoic of the Somerset coast. Journal of Structural Geology 21 (5), 493–509.
Kim, Y.-S., Andrews, J.R., Sanderson, D.J., 2001. Reactivated strike-slip faults: examples from north Cornwall, UK. Tectonophysics 340 (3-4), 173–194.
Lisle, R.J., Srivastava, D.C., 2004. Test of the frictional reactivation theory for faults and validity of fault-slip analysis. Geology 32 (7), 569–572.
McClay, K.R., 1990. Extensional fault systems in sedimentary basins: a review of analogue model studies. Marine and Petroleum Geology 7 (3), 206–233.
Meisling, K.E., Cobbold, P.R., Mount, V.S., 2001. Segmentation of an obliquely rifted margin, Campos and Santos basins, southeastern Brazil. American Association of Petroleum Geologists Bulletin 85 (11), 1903–1924.
Meyer, V., Nicol, A., Childs, C., Walsh, J.J., Watterson, J., 2002. Progressive localisation of strain during the evolution of a normal fault population. Journal of Structural Geology 24 (8), 1215–1231.
Mohriak, W.U., Palagi, P.R., Mello, M.R., 1998. Tectonic evolution of South Atlantic salt basins. American Association of Petroleum Geologists Bulletin 82 (10), 1945.
Muir Wood, R., Mallard, D.J., 1992. When is a fault 'extinct'? Journal of the Geological Society London 149 (2), 251–256.
Nicol, A., Walsh, J., Berryman, K., Nodder, S., 2005. Growth of a normal fault by the accumulation of slip over millions of years. Journal of Structural Geology 27 (2), 327–342.
Ojeda, H.A.O., 1982. Structural framework, stratigraphy, and evolution of Brazilian Marginal Basins. American Association of Petroleum Geologists Bulletin 66 (6), 732–749.
Parker, T.J., McDowell, A.N., 1951. Scale models as guide to interpretation of salt-dome faulting. American Association of Petroleum Geologists Bulletin 35, 2076–2086.
Paton, D.A., 2006. Influence of crustal heterogeneity on normal fault dimensions and evolution: southern South Africa extensional system. Journal of Structural Geology 28 (5), 868–886.
Peacock, D.C.P., Sanderson, D.J., 1994. Geometry and development of relay ramps in normal fault systems. American Association of Petroleum Geologists Bulletin 78 (2), 147–165.
Petersen, K., Clausen, O.R., Korstgard, J.A., 1992. Evolution of a salt-related listric growth fault near the d-1 well, block 5605, Danish North Sea: displacement history and salt kinematics. Journal of Structural Geology 14 (5), 565–577.
Richard, P., Krantz, R.W., 1991. Experiments on fault reactivation in strike-slip mode. Tectonophysics 188 (1-2), 117–131.
Rodger, M., Watts, A.B., Greenroyd, C.J., Peirce, C., Hobbs, R.W., 2006. Gravity anomalies, crustal structure, and flexure at the NE Brazil rifted continental margin. Geophysical Research Abstract 8, 07260.
Scott, D.R., Marone, C.J., Sammis, C.G., 1994. The apparent friction of granular fault gouge in sheared layers. Journal of Geophysical Research 99 (B4), 7231–7246.
Sibson, R.H., 1981. Fluids flow accompanying faulting, field evidence and models, in: Simpson, D.W., Richards, P.G. (Eds.), Earthquake Prediction, an International Review. American Geophysical Union Maurice Erwing Series vol. 4, 593–603.
Sibson, R.H., 1985. A note on fault reactivation. Journal of Structural Geology 7 (6), 751–754.
Vendeville, B.C., Jackson, M.P.A., 1992. The rise of diapirs during thin-skinned extension. Marine and Petroleum Geology 9 (4), 331–354.
Vetel, W., Le Gall, B., Walsh, J.J., 2005. Geometry and growth of an inner rift fault pattern: the Kino Sogo Fault Belt, Turkana Rift (North Kenya). Journal of Structural Geology 27 (12), 2204–2222.
Walsh, J.J., Watterson, J., 1988. Analysis of the relationship between displacements and dimensions of faults. Journal of Structural Geology 10 (3), 239–247.
Walsh, J.J., Nicol, A., Childs, C., 2002. An alternative model for the growth of faults. Journal of Structural Geology 24, 1669–1675.
Wendlandt, E.A., Shelby, T.H., Bell, J.S., 1946. Hawkins field, Wood County, Texas. American Association of Petroleum Geologists Bulletin 30, 1830–1856.
White, S.H., Bretan, P.G., Rutter, E.H., 1986. Fault-zone reactivation: kinematics and mechanisms. Philosophical Transactions of the Royal Society of London A317, 81–97.
Wilkins, S.J., Gross, M.R., 2002. Normal fault growth in layered rocks at Split Mountain, Utah: influence of mechanical stratigraphy on dip linkage, fault restriction and fault scaling. Journal of Structural Geology 24 (9), 1413–1429.
Withjack, M.O., Scheiner, C., 1982. Fault patterns associated with domes – an experimental and analytical study. American Association of Petroleum Geologists Bulletin 66 (3), 302–316.